Continuum Mech. Thermodyn.
DOI 10.1007/s00161-009-0115-3

ORIGINAL ARTICLE

P. Taheri · A. S. Rana · M. Torrilhon · H. Struchtrup

Macroscopic description of steady and unsteady rarefaction effects in boundary value problems of gas dynamics

Received: 21 April 2009 / Accepted: 24 September 2009

Abstract Four basic flow configurations are employed to investigate steady and unsteady rarefaction effects in monatomic ideal gas flows. Internal and external flows in planar geometry, namely, viscous slip (Kramer's problem), thermal creep, oscillatory Couette, and pulsating Poiseuille flows are considered. A characteristic feature of the selected problems is the formation of the Knudsen boundary layers, where non-Newtonian stress and non-Fourier heat conduction exist. The linearized Navier–Stokes–Fourier and regularized 13-moment equations are utilized to analytically represent the rarefaction effects in these boundary-value problems. It is shown that the regularized 13-moment system correctly estimates the structure of Knudsen layers, compared to the linearized Boltzmann equation data.

Keywords Kinetic theory of gases · Rarefied gas dynamics · Moment method · Knudsen boundary layers · Velocity slip and surface accommodation · Kramer's problem · Thermal creep flow · Oscillatory Couette flow · Pulsating Poiseuille flow

PACS 51.10.+y · 47.45.−n · 47.10.ab · 05.70.Ln · 47.45.Gx · 83.85.Vb

1 Introduction

In rarefied conditions, particle-based gas dynamics must be used to accurately describe the complicated transport phenomena in gaseous flows [1]. Complication of the transport field in dilute gas flows is due to the coexistence of non-equilibrium effects [2]. Kinetic gas theory can describe these non-equilibrium effects by numerical solutions of the kinetic Boltzmann equation, which however, are quite expensive.

Once a microscopic kinetic equation, e.g., the Boltzmann equation, is given, it is possible to derive the corresponding macroscopic transport equations. This is done by reducing the degrees of freedom of the velocity distribution function, that is the main variable in the kinetic equation, to the degrees of freedom of a finite set of macroscopic variables. The Chapman-Enskog expansion [3] and Grad's moment expansion [4,5] are the classical methods to extract hydrodynamic-like equations from the Boltzmann equation.

The Chapman-Enskog method replaces the velocity distribution function in the Boltzmann equation by its expansion in the Knudsen number, Kn. This leads to explicit expressions for heat-flux vector q_i, and stress tensor σ_{ij} as derivatives of the hydrodynamic variables —density ρ, temperature θ, and velocity v_i. Through a standard procedure, the Euler and Navier–Stokes–Fourier (NSF) equations follow from the zeroth- and first-order expansions, while the second- and third-order expansions yield the Burnett and super-Burnett equations, respectively [3].

P. Taheri (✉) · A. S. Rana · H. Struchtrup
Department of Mechanical Engineering, University of Victoria, Victoria, BC V8W 3P6, Canada
E-mail: peymant@uvic.ca

M. Torrilhon
Seminar for Applied Mathematics, ETH Zürich, Zürich 8092, Switzerland

Published online: 23 October 2009

Attempts at solving the Burnett-type equations have uncovered many physical and numerical difficulties. As proved in [6,7], the classical Burnett equations are vulnerable to instabilities, and in many cases give unphysical results. Consequently, several modified versions of these equations are proposed [8–12], aiming to stabilize them. Furthermore, it is important to highlight the lack of any systematic approach to derive boundary conditions for the Burnett-type equations, which requires evaluation of higher-order derivatives of the primary quantities on the boundary.

Quite differently compared to the Chapman-Enskog method, in the Grad's moment method the velocity distribution function is constructed by an expansion of the Maxwellian into Hermite polynomials [4,5]. The moments of the distribution function construct the list of macroscopic quantities, and the set of macroscopic quantities can be expanded based on the approximated polynomial. In Grad-type equations, the moment equations which are obtained from the Boltzmann equation govern the evolution of the moments. The advantage of Grad's method of moments is to avoid those instabilities that are inherent in the Chapman-Enskog method.

For the Maxwellian, the Grad's method corresponds to a five-moment system, which is equivalent to the Euler equations through $\mathcal{O}(Kn^0)$, governing the evolution of five equilibrium moments $\{\rho, \theta, v_i\}$ in inviscid flows without heat conduction. In Grad's classical 13-moment system the variables are extended to include the heat-flux vector and stress tensor. This hierarchy in the moment method continues with 26, 45, 71, 105, 148, ... moment systems, which yield to larger and larger systems [13].

According to the Chapman-Enskog method the Navier–Stokes–Fourier equations are first-order in the Knudsen number $\mathcal{O}(Kn^1)$, hence, they are appropriate only for processes in vicinity of the equilibrium state. The Navier–Stokes–Fourier system can be viewed as the regularized version of the Euler equations. This means that the first-order non-equilibrium quantities (Navier–Stokes shear stress and Fourier heat flux), which exist in the 13-moment system, are included in the 5-moment system (Euler equations) only to some extent. These first-order contributions are expressed by means of space derivatives of the equilibrium variables. Nevertheless, higher-order rarefaction effects remain intangible for the Navier–Stokes–Fourier system.

The regularized 13-moment (R13) system is a regularized version of the classical Grad's 13-moment equations [13–15], suitable for flow simulation in the transition regime, $Kn \leqslant 1$. The R13 system includes third-order moments which exist in the 26-moment system, hence, they are comparable to super-Burnett equations. In contrast to Grad's 13-moment system, the R13 equations yield continuous shock structures at all Mach numbers [16], and correctly predict the formation of Knudsen boundary layers in fundamental boundary value problems for microflows [17–23].

Recently, a computational strategy to obtain boundary conditions for high-order moments was introduced [20,24]. Availability of boundary conditions provides a great potential for application of the R13 equations in practical problems. At the starting point, classical shear-driven and force-driven micro-channels flows were studied with the R13 equations and their boundary conditions [20–22]. The simulations proved that the R13 equations can predict all rarefaction effects which are observed in Direct Simulation Monte Carlo (DSMC) and the Boltzmann equation solutions. These rarefaction effects include discontinuity of velocity and temperature on the boundary, Knudsen layers, characteristic dip in the temperature profile and Knudsen Paradox in Poiseuille flow. Particularly, in [22] it is shown that even analytical solutions of the R13 equations can approximate extensive numerical solutions of the Boltzmann equation in the transition regime. This motivated further flow simulations, including thermally induced flows [23]. In the present article, rarefaction effects in a collection of steady and unsteady boundary value problems are investigated. Steady state external flows in slab geometry, namely, viscous slip and thermal creep flows, along with periodically unsteady internal flows, "Oscillatory Couette" and "Pulsating Poiseuille" flows are considered as generic models.

At the boundary, the interaction of the gas molecules with the surface leads to discontinuities in the particles' velocity distribution. On the macroscopic scale, these discontinuities yield a non-equilibrium layer adjacent to the boundary, the Knudsen boundary layer. In this article, simple plane flows are employed to investigate the formation of Knudsen boundary layers in selected boundary value problems. NSF and R13 systems in their linear forms are adapted to solve the problems analytically, and the results are compared to solutions of the linearized Boltzmann equation and DSMC data. For unsteady problems with harmonic oscillations in shear force and body force, interaction of rarefaction effects, and unsteady viscous effects are apparent through the presented analytical solutions.

2 Classical and extended macroscopic transport equations

2.1 Navier–Stokes–Fourier: classical hydrodynamics

All macroscopic transport equations are based on the fundamental conservation laws for mass, momentum, and total energy densities,

$$\begin{aligned} \frac{\partial \rho}{\partial t} + \frac{\partial \rho v_k}{\partial x_k} &= 0, \\ \frac{\partial \rho v_i}{\partial t} + \frac{\partial \left(\rho v_i v_k + p_{ik}\right)}{\partial x_k} &= \rho g_i, \\ \frac{\partial \rho e}{\partial t} + \frac{\partial \left(\rho e v_k + v_i p_{ik} + q_k\right)}{\partial x_k} &= \rho g_i v_i, \end{aligned} \tag{2.1}$$

where t and x_k are the time and spatial position. The quantities ρ, v_k, p_{ik}, g_i, e, and q_k denote mass density, velocity vector, pressure tensor, body-force vector, (total) energy density, and heat-flux vector, respectively, with

$$p_{ik} = p\delta_{ik} + \sigma_{ik} \quad \text{and} \quad e = u + \frac{1}{2}v^2.$$

Here, δ_{ik} is the Kronecker delta, $p = p_{kk}/3$ is the pressure, and $\sigma_{ik} = p_{\langle ik \rangle}$ is the symmetric and trace-free stress tensor, i.e., the non-equilibrium part of the pressure tensor. Indices inside angular brackets indicate trace-free symmetric tensors, e.g., the trace-free part of the matrix A_{ij} is $A_{\langle ij \rangle} = \left(A_{ij} + A_{ji}\right)/2 - A_{kk}\delta_{ij}/3$, and similarly for three indices, see [13]. The internal energy density is denoted by u, and, since we consider monatomic ideal gases, $p = \rho\theta$ and $u = 3\theta/2$ hold as the equations of state, where θ is the temperature in energy units ($\theta = \mathcal{R}T$, where $\mathcal{R}$ is the gas constant and T is thermodynamic temperature).

The laws of Navier and Stokes for viscosity, and Fourier's law for heat conduction read

$$\sigma_{ik}^{(\mathrm{NSF})} = -2\mu \frac{\partial v_{\langle i}}{\partial x_{k\rangle}} \quad \text{and} \quad q_i^{(\mathrm{NSF})} = -\frac{15}{4}\mu \frac{\partial \theta}{\partial x_i}, \tag{2.2}$$

where $\mu = \mu(\theta)$ is the viscosity, and $15\mathcal{R}\mu/4$ is the heat conductivity for Maxwell molecules [13]. In classical hydrodynamics (2.2) is utilized as constitutive relation in order to provide closure for (2.1).

The well-known Euler equations describe equilibrium flows, where $\sigma_{ik} = q_i = 0$. For these inviscid flows without heat conduction, the conservation laws (2.1) only contain the equilibrium quantities $\{\rho, v_i, \theta\}$.

The hierarchy in Grad's moment method begins with the 5-moment theory that is equivalent to the Euler equations, governing the evolution of the five equilibrium quantities. The closure given in (2.2) introduces the lowest-order non-equilibrium moments, i.e., Navier–Stokes stress and Fourier heat flow, in terms of the equilibrium moments. Inclusion of stress and heat flux in the balance laws (2.1), changes the hyperbolic Euler equations to the NSF equations which are of mixed parabolic–hyperbolic type. These corrections are taken from the 13-moment theory, which holds the second place in the moment hierarchy. Accordingly, the NSF system can be addressed as regularization of the Euler equations, using the next higher-order moments.

By means of the standard expansion in the Knudsen number, the Chapman-Enskog expansion [3], it is straightforward to show that the Euler equations represent the zeroth-order expansion; while the first-order expansion yields to the NSF equations. Hence, the NSF equations can describe processes in the vicinity of the equilibrium state.

2.2 Regularized 13-moment theory: extended hydrodynamics

Burnett-type equations which are extended continuum models, obtained from the Chapman-Enskog expansion, provide corrections to the Navier–Stokes and Fourier laws. These corrections appear as high-order derivatives of the primary variables in the conservation laws, $\{\rho, v_i, \theta\}$.

On the other hand, Grad-type equations, which go beyond hydrodynamics by expansion of the moment equations, add higher-order moments to their variable list, and require closure based on the extended variables. In the 13-field theory, components of heat-flux vector and stress tensor besides the equilibrium variables form the list of variables, while full balance equations for heat-flux vector and stress tensor are included in

the system. The classical Grad's 13-moment equations [4,5] are second-order in Knudsen number, and their regularization [14] which includes elements of the 26-moment system, promotes them to be of $\mathcal{O}(Kn^3)$.

The equations for heat-flux vector and stress tensor in the regularized 13-moment system are their respective moment equations [4,5,13–15],

$$\begin{aligned}&\frac{\partial q_i}{\partial t}+\frac{\partial v_k q_i}{\partial x_k}+\underline{\frac{5}{2}\frac{\partial \theta}{\partial x_k}(p\delta_{ik}+\sigma_{ik})}+\theta\frac{\partial \sigma_{ik}}{\partial x_k}-\frac{\theta\sigma_{ik}}{\rho}\frac{\partial \rho}{\partial x_k}+\frac{2}{5}\left(q_k\frac{\partial v_k}{\partial x_i}+q_i\frac{\partial v_k}{\partial x_k}\right)\\&+\frac{7}{5}q_k\frac{\partial v_i}{\partial x_k}+\frac{1}{2}\frac{\partial R_{ik}}{\partial x_k}+\frac{1}{6}\frac{\partial \Delta}{\partial x_i}+m_{ijk}\frac{\partial v_j}{\partial x_k}-\frac{\sigma_{ij}}{\rho}\frac{\partial \sigma_{jk}}{\partial x_k}=\underline{-\frac{2}{3}\frac{p}{\mu}q_i},\end{aligned}\tag{2.3}$$

and

$$\frac{\partial \sigma_{ij}}{\partial t}+\frac{\partial v_k\sigma_{ij}}{\partial x_k}+\frac{4}{5}\frac{\partial q_{\langle i}}{\partial x_{j\rangle}}+\underline{2p\frac{\partial v_{\langle i}}{\partial x_{j\rangle}}}+2\sigma_{k\langle i}\frac{\partial v_{j\rangle}}{\partial x_k}+\frac{\partial m_{ijk}}{\partial x_k}=\underline{-\frac{p}{\mu}\sigma_{ij}}.\tag{2.4}$$

The moment equations (2.3, 2.4) contain the additional higher moments Δ, R_{ik}, and m_{ijk}. In Grad's classical 13-moment theory [4,5] these vanish, $\Delta = R_{ik} = m_{ijk} = 0$, while the regularization procedure gives [13–15]

$$\begin{aligned}\Delta&=-\frac{\sigma_{ij}\sigma_{ij}}{\rho}-12\frac{\mu}{p}\left(\theta\frac{\partial q_k}{\partial x_k}+\frac{5}{2}q_k\frac{\partial \theta}{\partial x_k}-\theta q_k\frac{\partial \ln\rho}{\partial x_k}+\theta\sigma_{kl}\frac{\partial v_k}{\partial x_l}\right),\\R_{ij}&=-\frac{4}{7}\frac{\sigma_{k\langle i}\sigma_{j\rangle k}}{\rho}-\frac{24}{5}\frac{\mu}{p}\left(\theta\frac{\partial q_{\langle i}}{\partial x_{j\rangle}}+q_{\langle i}\frac{\partial \theta}{\partial x_{j\rangle}}-\theta q_{\langle i}\frac{\partial \ln\rho}{\partial x_{j\rangle}}+\frac{10}{7}\theta\sigma_{k\langle i}S_{j\rangle k}\right),\\m_{ijk}&=-2\frac{\mu}{p}\left(\theta\frac{\partial \sigma_{\langle ij}}{\partial x_{k\rangle}}-\theta\sigma_{\langle ij}\frac{\partial \ln\rho}{\partial x_{k\rangle}}+\frac{4}{5}q_{\langle i}\frac{\partial v_j}{\partial x_{k\rangle}}\right),\end{aligned}\tag{2.5}$$

with $S_{jk} = \partial v_{\langle j}/\partial x_{k\rangle}$.

We emphasize that Eqs. 2.3–2.5 are derived for Maxwell molecules [13–15]. In order to compare the solution of the above equations to other kinetic solutions, proper scaling needs to be applied between the underlying kinetic models. For example, comparison with the BGK model requires different factors in the above equations, see the Appendix.

The constitutive equations in (2.5) introduce second-order derivatives into the transport equations (2.3, 2.4), which lead to their regularization. In particular these regularizing terms lead to continuous shock structures [16]. Similarly, Navier–Stokes and Fourier laws (2.2) provide regularization for Euler equations.

In the limit of small Knudsen numbers, Eqs. 2.3, 2.4 reduce to the Navier–Stokes and Fourier laws (2.2), that is only the underlined terms remain [13,14]. Recall that in the 5-moment theory these underlined terms are used for regularization of the Euler equations.

3 General statement of the problems

3.1 Steady problems: viscous slip and thermal creep flows

The problem of viscous (velocity) slip, also called Kramer's problem, concerns half-space ($x_2 > 0$) gas flow over a flat solid surface at $x_2 = 0$, see Fig. 1 (left). The temperature of the surface θ_W is kept constant at θ_0. Far from the wall the temperature and density of the gas are constant (θ_0 and ρ_0), however, there is a gas flow parallel to the wall, whose velocity is a linear function of x_2; $\partial_{x_2} v_1 = A$ with A as the constant velocity gradient in the bulk. This flow can be considered as Couette flow in parallel-plate micro-channels, where the distance between the channel walls is infinite. Note that the relative velocity of the plates in Couette flow is equivalent to the prescribed constant velocity gradient of bulk flow in the Kramer's problem [20–22].

While in the viscous slip flow the surface temperature is uniform, in thermal creep flow a streamwise constant temperature gradient $\partial_{x_1}\theta = B$ is applied in the surface, Fig. 1 (right). This boundary treatment induces a tangential velocity in the gas close to the surface such that the gas flows in direction of the temperature gradient, i.e., from cold to hot. Also, it is assumed that the length of the plate, L, is sufficiently large that the creep layer is fully developed, this implies that the same temperature gradient is established in the gas, and far from the surface the pressure is constant [23,25].

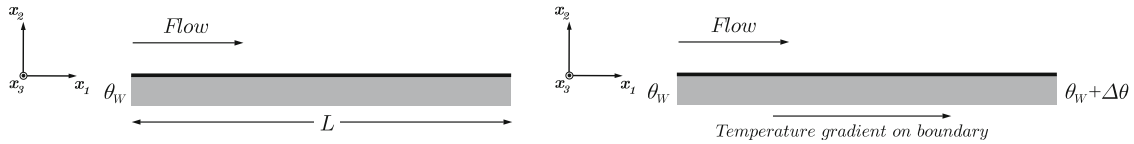

Fig. 1 *Left* Viscous slip flow, known as Kramer's problem, is one-dimensional viscous flow over a stationary flat wall, where temperatures of the wall θ_W and flow are the same. In the bulk flow, there is a constant velocity gradient normal to the wall in x_2 direction, which sweeps the gas particles over the surface. *Right* In thermal creep flow a non-uniform temperature distribution in a flat plate induces a tangential velocity in the adjacent gas. This thermally induced flow is in the direction of the temperature gradient, i.e., in the opposite direction of heat flow

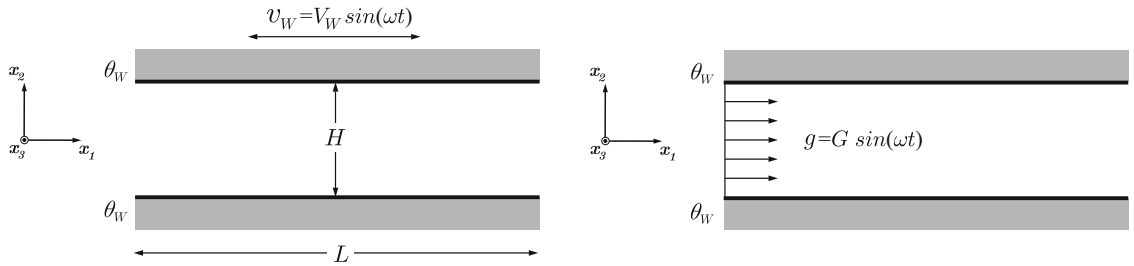

Fig. 2 *Left* In oscillatory Couette flow a viscous fluid between two parallel plates at temperature θ_W, separated by distance H, is excited by lateral oscillations of the top plate. *Right* In pulsating Poiseuille flow plates are stationary and a harmonically pulsating body force is applied. In both problems one-dimensional flows are considered

Thermal creep flow over a plate can be observed as transpiration flow in parallel-plate micro-channels, where the channel height is finite [23,25]. In the case of transpiration flow in micro-channels, temperature gradients on the walls induce a tangential velocity in the interior gas close to the walls. In moderately rarefied gases, this thermally induced velocity initiates within a thin boundary layer. The thickness of this creep layer is proportional to the Knudsen number. In sufficiently long channels, the velocity gradient within the creep layer fills the channel width as a result of shear stress diffusion.

3.2 Unsteady problems: oscillatory Couette and pulsating Poiseuille flows

In oscillatory Couette flow, the gas is confined in a slit between two infinite parallel plates, where one of the plates (upper plate) oscillates harmonically in its own plane, and the other plate is stationary, see Fig. 2 (left). The velocity of the oscillatory wall is $v_W = V_W \sin(\omega t)$, where ω and V_W are constant frequency and velocity amplitude of the exerted oscillations. The plates are parallel in direction x_1, separated by distance H, located on $x_2 = \pm H/2$. Both plates are assumed to be isothermal at temperature θ_0.

This flow configuration can be viewed as the limiting case of the classical Stokes' second problem in fluid mechanics, where a semi-infinite expanse of a viscous fluid is bounded by a laterally oscillating flat surface [26]. In the Stokes' problem the plate oscillations propagate into the infinite expanse of the surrounding gas. In the oscillatory Couette flow the range of propagation is limited between the walls.

The viscous damping mechanism in oscillatory shear-driven flows is applied in many MEMS designs, including resonant sensors/actuators, microfilters, microaccelerometers, and microbearings [27].

In pulsating Poiseuille flow both plates of the channel are at rest and a homogeneous oscillating force is driving the process, see Fig. 2 (right). We assume the force to be $g = G \sin(\omega t)$ with amplitude G and frequency ω, acting in x_1 direction. The rest of the setup is equivalent to the oscillatory Couette case. Standard Poiseuille flow without time-depending force is known to exhibit non-intuitive behavior like the Knudsen Paradox for small channel widths, see [1,25]. Hence, we expect interesting phenomena for the pulsating case.

3.3 Assumptions

In all the above-mentioned problems monatomic ideal gas flows are assumed. The flows are independent of the direction x_3, as sufficiently wide plates are considered, which construct a rectangular channel with a large cross-sectional aspect ratio. The plates act as thermal reservoirs, and are impermeable.

We will consider flows in the linear regime, where the viscous slip, oscillatory Couette, and pulsating Poiseuille flows will turn out to be isothermal. This means that the plates and gas remain at the same temperature θ_0, since viscous heating effects are negligible. In these problems a unidirectional velocity field parallel to the plates is allowed, $v_i = \{v_1(x_2), 0, 0\}$, and flow parameters are independent of the stream direction x_1, $\partial_{x_1} = 0$.

Thermal creep flow is different from the other flow configurations. Owing to the temperature/density gradient, the constant pressure creep flow is not isothermal. Hence, unidimensional flow is not assured, and the velocity field is two-dimensional, $v_i = \{v_1(x_1, x_2), v_2(x_1, x_2), 0\}$. Nevertheless, we realized when the streamwise temperature gradient is small, the compressibility effects can be discarded, which leads to $v_2 = 0$. In the following calculations for the creep flow, we superimpose a unidirectional velocity field. It will be shown that this assumption is consistent with the linear results.

Based on the above discussion the velocity vector, heat-flux vector, and stress tensor for all the considered flows here reduce to

$$\begin{aligned} v_i &= \{v_1(x_2), 0, 0\}, \\ q_i &= \{q_1(x_2), q_2(x_2), 0\}, \\ \sigma_{ij} &= \begin{bmatrix} \sigma_{11}(x_2) & \sigma_{12}(x_2) & 0 \\ \sigma_{12}(x_2) & \sigma_{22}(x_2) & 0 \\ 0 & 0 & -\sigma_{11}(x_2) - \sigma_{22}(x_2) \end{bmatrix}. \end{aligned} \tag{3.1}$$

4 Linearized and dimensionless equations for parallel-plate micro-channel flows

In our analysis, we employ the linear forms of the Navier–Stokes–Fourier and R13 equations. Linearization is allowed for small gradients in the half-space problems, and small amplitudes in the oscillatory problems. The merit of linearization is brevity of the equations, which makes the analytical solution accessible. Indeed, coupling between variables are discarded through the linearized equations; for instance, viscous heating effects which link the velocity and temperature fields is not included in the linearized equations.

Knudsen layers which are interesting rarefaction effects in our considered problems, can be computed from the linearized equations. In slow rarefied flows, e.g., microflows, Knudsen layers are dominant rarefaction effects. Inclusion of non-linear terms in the equations leads to more accuracy in prediction of Knudsen layers and bulk effects, which of course demands numerical solution. Note, however, some non-linear effects can be described in analytical solutions [22].

The reference equilibrium state is defined by $\{\rho_0, \theta_0, v_i^0\}$, which is used for non-dimensionalization and linearization. Dimensionless density and temperature are defined as their deviations from the reference equilibrium state, $\tilde{\rho} = \rho/\rho_0 - 1$, and $\tilde{\theta} = \theta/\theta_0 - 1$. Also, the isothermal speed of sound, $\sqrt{\theta_0}$, is employed as the velocity scale.

In the half-space problems, i.e., viscous slip and thermal creep flows, the molecular mean free path in equilibrium λ_0 is assigned as the characteristic length scale to define the dimensionless position vectors $\tilde{x_1} = x_1/\lambda_0$ and $\tilde{x_2} = x_2/\lambda_0$. Moreover, the dimensionless time is defined by $\tilde{t} = t/t_0$, with $t_0 = \lambda_0/\sqrt{\theta_0}$.

In the unsteady channel flows, the height of the channel H defines the macroscopic length scale, $\tilde{x_2} = x_2/H$.

The rest of the variables in proper dimensionless form are

$$\begin{aligned} &\tilde{g}_i = \frac{H}{\theta_0} g_i, \quad \tilde{v}_i = \frac{v_i}{\sqrt{\theta_0}}, \quad \tilde{\sigma}_{ij} = \frac{\sigma_{ij}}{\rho_0 \theta_0}, \quad \tilde{q}_i = \frac{q_i}{\rho_0 \sqrt{\theta_0}^3}, \\ &\tilde{\Delta} = \frac{\Delta}{\rho_0 \theta_0^2}, \quad \tilde{R}_{ij} = \frac{R_{ij}}{\rho_0 \theta_0^2}, \quad \tilde{m}_{ijk} = \frac{m_{ijk}}{\rho_0 \sqrt{\theta_0}^3}. \end{aligned} \tag{4.1}$$

Furthermore, $\tilde{\mu} = \mu/\mu_0 - 1$ is the dimensionless viscosity deviation with $\mu_0 = \mu(\theta_0)$. In the reference state, the moments assume the values $\rho_0 = \theta_0 = p_0 = 1$, and $v_i^0 = \sigma_{ij}^0 = q_i^0 = \Delta_0 = R_{ij}^0 = m_{ijk}^0 = 0$. Accordingly, deviations vanish in the reference equilibrium state, i.e., $\tilde{\rho} = \tilde{\theta} = \tilde{\mu} = 0$.

In the standard linearization, only terms that are linear in deviations from the ground equilibrium state are included within the equations, which leads to decoupling of the equations for velocity and temperature. Accordingly, $\tilde{p} = 1 + \tilde{\rho} + \tilde{\theta}$ is the linearized and dimensionless equation of state for the ideal gas. This implies that in the thermal creep flow, where pressure is constant along the plate, $\partial_{\tilde{x}_1}\tilde{\theta} = -\partial_{\tilde{x}_1}\tilde{\rho} = \text{constant}$.

For the considered flow geometries, illustrated in Figs. 1 and 2, Eqs. 2.1, 2.3, 2.4 in their linear and dimensionless format reduce to the velocity problem

$$\frac{\partial \tilde{v}_1}{\partial \tilde{t}} + \frac{\partial \tilde{\sigma}_{12}}{\partial \tilde{x}_2} = \tilde{g}_1, \tag{4.2a}$$

$$\frac{\partial \tilde{\sigma}_{12}}{\partial \tilde{t}} + \frac{2}{5}\frac{\partial \tilde{q}_1}{\partial \tilde{x}_2} + \frac{\partial \tilde{v}_1}{\partial \tilde{x}_2} + \frac{\partial \tilde{m}_{122}}{\partial \tilde{x}_2} = -\frac{1}{Kn}\tilde{\sigma}_{12}, \tag{4.2b}$$

$$\frac{\partial \tilde{q}_1}{\partial \tilde{t}} + \frac{5}{2}\frac{\partial \tilde{\theta}}{\partial \tilde{x}_1} + \frac{\partial \tilde{\sigma}_{12}}{\partial \tilde{x}_2} + \frac{1}{2}\frac{\partial \tilde{R}_{12}}{\partial \tilde{x}_2} = -\frac{2}{3}\frac{1}{Kn}\tilde{q}_1, \tag{4.2c}$$

the temperature problem

$$\frac{3}{2}\frac{\partial \tilde{\theta}}{\partial \tilde{t}} + \frac{\partial \tilde{q}_2}{\partial \tilde{x}_2} = 0, \tag{4.3a}$$

$$\frac{\partial \tilde{\sigma}_{22}}{\partial \tilde{t}} + \frac{2}{3}\frac{\partial \tilde{q}_2}{\partial \tilde{x}_2} + \frac{\partial \tilde{m}_{222}}{\partial \tilde{x}_2} = -\frac{1}{Kn}\tilde{\sigma}_{22}, \tag{4.3b}$$

$$\frac{\partial \tilde{q}_2}{\partial \tilde{t}} + \frac{5}{2}\frac{\partial \tilde{\theta}}{\partial \tilde{x}_2} + \frac{\partial \tilde{\sigma}_{22}}{\partial \tilde{x}_2} + \frac{1}{2}\frac{\partial \tilde{R}_{22}}{\partial \tilde{x}_2} + \frac{1}{6}\frac{\partial \tilde{\Delta}}{\partial \tilde{x}_2} = -\frac{2}{3}\frac{1}{Kn}\tilde{q}_2, \tag{4.3c}$$

and the density problem

$$\frac{\partial \tilde{\rho}}{\partial \tilde{x}_2} + \frac{\partial \tilde{\theta}}{\partial \tilde{x}_2} + \frac{\partial \tilde{\sigma}_{22}}{\partial \tilde{x}_2} = 0, \tag{4.4a}$$

$$\frac{\partial \tilde{\sigma}_{11}}{\partial \tilde{t}} - \frac{4}{15}\frac{\partial \tilde{q}_2}{\partial \tilde{x}_2} + \frac{\partial \tilde{m}_{112}}{\partial \tilde{x}_2} = -\frac{1}{Kn}\tilde{\sigma}_{11}, \tag{4.4b}$$

where the following linear and dimensionless constitutive relations (2.5) are required

$$\begin{gathered}\tilde{\Delta} = -12\,Kn\frac{\partial \tilde{q}_2}{\partial \tilde{x}_2}, \quad \tilde{R}_{12} = -\frac{12}{5}Kn\frac{\partial \tilde{q}_1}{\partial \tilde{x}_2}, \quad \tilde{R}_{22} = -\frac{16}{5}Kn\frac{\partial \tilde{q}_2}{\partial \tilde{x}_2}, \\ \tilde{m}_{112} = -\frac{2}{3}Kn\left(\frac{\partial \tilde{\sigma}_{11}}{\partial \tilde{x}_2} - \frac{2}{5}\frac{\partial \tilde{\sigma}_{22}}{\partial \tilde{x}_2}\right), \quad \tilde{m}_{122} = -\frac{16}{15}Kn\frac{\partial \tilde{\sigma}_{12}}{\partial \tilde{x}_2}, \quad \tilde{m}_{222} = -\frac{6}{5}Kn\frac{\partial \tilde{\sigma}_{22}}{\partial \tilde{x}_2}.\end{gathered} \tag{4.5}$$

Here, Kn is the Knudsen number, defined as the ratio of the mean free path at the reference equilibrium state λ_0 to the characteristic length $\mathcal{L}$

$$Kn = \frac{\lambda_0}{\mathcal{L}}, \quad \text{where} \quad \begin{cases} Kn = 1, & \text{for the half-space flows} \\ Kn = \frac{\mu_0}{\rho_0\sqrt{\theta_0}H}, & \text{for the channel flows.} \end{cases} \tag{4.6}$$

For briefness, governing equations for the considered boundary value problems are unified in (4.2)–(4.5). In the steady problems, time derivative terms must be excluded from the equations; $\tilde{g}_1$ is zero except for the pulsating Poiseuille flow; $\partial_{\tilde{x}_1}\tilde{\theta}$ is zero except for the creep flow.

The equations in the velocity problem govern the evolution of $\{\tilde{v}_1, \tilde{q}_1, \tilde{\sigma}_{12}\}$ in space and time. Note that derivatives with respect to time and space exist in each equation. Analogously, the three equations in the temperature problem describe temporal and spatial evolution for $\{\tilde{\theta}, \tilde{q}_2, \tilde{\sigma}_{22}\}$. In the density problem there are two equations for two unknown variables $\{\tilde{\rho}, \tilde{\sigma}_{11}\}$, however, the temperature problem solution is required.

If we assume two dimensional flows, then $\tilde{v}_2$ is responsible for the redistribution of mass in the cross section, i.e., for constant $\tilde{x}_1$. In our problems, we assumed $\tilde{v}_2 = 0$. This implies that the redistribution of density cannot be described by the continuity equation. Instead, the density follows from the equation for $\tilde{v}_2$, i.e., the balance of momentum in x_2-direction, Eq. 4.4a, which describes the instantaneous change of density. For steady thermal creep flow, we shall further discuss the continuity equation in Sect. 7.2. For oscillatory Couette and Poiseuille flows in the linear regime, the velocity and temperature problems can be solved independently from density.

In the following, we only present solutions for the velocity problem. Temperature problem for viscous slip and oscillatory flows can be solved with the help of linearized boundary conditions. The required boundary

conditions for the temperature problem are presented in Sect. 6. The solution of the linear temperature problem gives

$$\tilde{q}_2 = 0, \qquad \tilde{\sigma}_{22} = 0, \qquad \tilde{\theta} = \theta_0,$$

that means the flows are isothermal.

Similarly, trivial solution for the density problem can be concluded from temperature solution and corresponding boundary conditions.

We emphasize that in the thermal creep flow, streamwise thermal effects can be described by the velocity problem, due to the one-dimensional velocity assumption.

5 The solutions

5.1 Viscous slip flow

For the steady state shear-driven flow over a flat surface the velocity problem (4.2) reduces to

$$\frac{\mathrm{d}\tilde{\sigma}_{12}}{\mathrm{d}\tilde{x}_2} = 0, \qquad \frac{2}{5}\frac{\mathrm{d}\tilde{q}_1}{\mathrm{d}\tilde{x}_2} + \frac{\mathrm{d}\tilde{v}_1}{\mathrm{d}\tilde{x}_2} = -\frac{1}{Kn}\tilde{\sigma}_{12}, \qquad \frac{6}{5}Kn\frac{\mathrm{d}^2\tilde{q}_1}{\mathrm{d}\tilde{x}_2^2} = \frac{2}{3}\frac{1}{Kn}\tilde{q}_1, \tag{5.1}$$

where $\tilde{R}_{12}$ and $\tilde{m}_{122}$ are substituted by the constitutive relations (4.5).

For the BGK model, the velocity problem takes the same form as (5.1), but different factors appear in the heat flux balance (see the Appendix for the BGK factors), so that

$$\frac{d\tilde{\sigma}_{12}}{d\tilde{x}_2} = 0, \qquad \frac{2}{5}\frac{d\tilde{q}_1}{d\tilde{x}_2} + \frac{d\tilde{v}_1}{d\tilde{x}_2} = -\frac{1}{Kn}\tilde{\sigma}_{12}, \qquad \frac{7}{5}Kn\frac{d^2\tilde{q}_1}{d\tilde{x}_2^2} = \frac{1}{Kn}\tilde{q}_1. \tag{5.2}$$

We continue with the BGK equations, since we shall compare our results with BGK Boltzmann data. The solution for (5.2) follows by integrating as

$$\tilde{\sigma}_{12} = \underline{\mathsf{C}_1}, \qquad \tilde{v}_1 = \underline{\mathsf{C}_4 - \frac{\tilde{\sigma}_{12}}{Kn}\tilde{x}_2} - \frac{2}{5}\tilde{q}_1, \qquad \tilde{q}_1 = \mathsf{C}_2\exp\left(\frac{\sqrt{5}}{\sqrt{7}\,Kn}\tilde{x}_2\right) + \mathsf{C}_3\exp\left(\frac{-\sqrt{5}}{\sqrt{7}\,Kn}\tilde{x}_2\right), \tag{5.3}$$

with C_1 to C_4 as the integrating constants, which need to be determined from boundary conditions.

The underlined terms represent the solution for the NSF equations. Note that both R13 and NSF systems yield constant shear stress, $\tilde{\sigma}_{12} = \mathsf{C}_1$. The term C_4 is the velocity slip, and $-\tilde{\sigma}_{12}\tilde{x}_2/Kn$ is the bulk solution. The NSF system predicts heat flux only in the direction of the temperature gradient, thus, it cannot predict the tangential heat flux $\tilde{q}_1$ in isothermal flows. Indeed, a heat flux in flow direction not driven by temperature gradient is a pure rarefaction effect [22] which lies beyond the capabilities of traditional hydrodynamics.

5.2 Thermal creep flow

In the steady state thermally induced flow over a flat wall, where $\tilde{g}_1 = 0$, the proper form of the velocity problem (4.2) is

$$\frac{\mathrm{d}\tilde{\sigma}_{12}}{\mathrm{d}\tilde{x}_2} = 0, \qquad \frac{2}{5}\frac{\mathrm{d}\tilde{q}_1}{\mathrm{d}\tilde{x}_2} + \frac{\mathrm{d}\tilde{v}_1}{\mathrm{d}\tilde{x}_2} = -\frac{1}{Kn}\tilde{\sigma}_{12}, \qquad \frac{5}{2}\beta - \frac{6}{5}Kn\frac{\mathrm{d}^2\tilde{q}_1}{\mathrm{d}\tilde{x}_2^2} = -\frac{2}{3}\frac{1}{Kn}\tilde{q}_1, \tag{5.4}$$

where $\partial_{\tilde{x}_1}\tilde{\theta} = \beta = B\lambda_0/\theta_0$ is the dimensionless streamwise temperature gradient.

For the BGK model, the velocity problem takes the same form as (5.4), but different factors appear in the heat flux balance (see the Appendix for the BGK factors),

$$\frac{\mathrm{d}\tilde{\sigma}_{12}}{\mathrm{d}\tilde{x}_2} = 0, \qquad \frac{2}{5}\frac{\mathrm{d}\tilde{q}_1}{\mathrm{d}\tilde{x}_2} + \frac{\mathrm{d}\tilde{v}_1}{\mathrm{d}\tilde{x}_2} = -\frac{1}{Kn}\tilde{\sigma}_{12}, \qquad \frac{5}{2}\beta - \frac{7}{5}Kn\frac{\mathrm{d}^2\tilde{q}_1}{\mathrm{d}\tilde{x}_2^2} = -\frac{1}{Kn}\tilde{q}_1, \tag{5.5}$$

Similar to the viscous slip problem, integrating (5.5) leads to

$$\tilde{\sigma}_{12} = \underline{\mathsf{C}_1}, \quad \tilde{v}_1 = \underline{\mathsf{C}_4 - \frac{\tilde{\sigma}_{12}}{Kn}\tilde{x}_2 - \frac{2}{5}\tilde{q}_1}, \quad \tilde{q}_1 = \underline{-\frac{5}{2}Kn\,\beta} + \mathsf{C}_2 \exp\left(\frac{\sqrt{5}}{\sqrt{7}\,Kn}\tilde{x}_2\right) + \mathsf{C}_3 \exp\left(\frac{-\sqrt{5}}{\sqrt{7}\,Kn}\tilde{x}_2\right). \tag{5.6}$$

The general solutions for viscous slip and thermal creep problems only differ in the heat-flux solution. In the creep flow, superposition of the Fourier's law and Knudsen layers construct the parallel heat flux. In the velocity solution, C_4 and the contribution of the Fourier's law represent the slip velocity (temperature-driven plug flow).

In (5.3) and (5.6), the exponential functions represent the Knudsen boundary layers. Similar to the analytical solutions in [18,21–23], these Knudsen layers can be written as hyperbolic sine and cosine functions.

5.3 Oscillatory Couette flow

For periodically unsteady shear-driven flow the time derivatives are retained within the governing Eq. 4.2, and the velocity problem assumes the form

$$\frac{\partial \tilde{v}_1}{\partial \tilde{t}} + \frac{\partial \tilde{\sigma}_{12}}{\partial \tilde{x}_2} = 0, \tag{5.7a}$$

$$\frac{\partial \tilde{\sigma}_{12}}{\partial \tilde{t}} + \frac{2}{5}\frac{\partial \tilde{q}_1}{\partial \tilde{x}_2} + \frac{\partial \tilde{v}_1}{\partial \tilde{x}_2} - \frac{16}{15}\mathrm{Kn}\frac{\partial^2 \tilde{\sigma}_{12}}{\partial \tilde{x}_2^2} = -\frac{1}{\mathrm{Kn}}\tilde{\sigma}_{12}, \tag{5.7b}$$

$$\frac{\partial \tilde{q}_1}{\partial \tilde{t}} + \frac{\partial \tilde{\sigma}_{12}}{\partial \tilde{x}_2} - \frac{6}{5}\mathrm{Kn}\frac{\partial^2 \tilde{q}_1}{\partial \tilde{x}_2^2} = -\frac{2}{3}\frac{1}{\mathrm{Kn}}\tilde{q}_1. \tag{5.7c}$$

The oscillation velocity at the upper wall is written in complex form as $v_W = V_W \exp(i\omega t)$, where $\Im[v_W] = V_W \sin(\omega t)$ indicates its imaginary part. As long as calculations involve only linear operations, we can omit the imaginary sign and proceed with the complex form, taking the imaginary part of the final result.

We introduce a dimensionless frequency W by writing

$$\sin(\omega t) = \sin\left(W\,\tilde{t}\right) = \sin\left(Kn\,St^2\,\tilde{t}\right), \tag{5.8}$$

with

$$St = H\left(\frac{\rho_0\,\omega}{\mu_0}\right)^{1/2}, \quad \text{and} \quad W = \omega\,t_0 = \frac{\omega\,H}{\sqrt{\theta_0}}. \tag{5.9}$$

The parameter St is the Stokes number (at the reference equilibrium state), which is also used in [28–31]. The Stokes number is defined as the ratio of shear diffusion time scale to the oscillation time scale, and represents the unsteady effects.

The long time solutions for (5.7) are expected as plane harmonic waves

$$\tilde{u}\left(\tilde{x}_2, \tilde{t}\right) = \mathcal{U}\exp\left[i\left(Kn\,St^2\,\tilde{t} - \tilde{k}\,\tilde{x}_2\right)\right], \quad \text{where} \quad \tilde{u} = \{\tilde{v}_1, \tilde{q}_1, \tilde{\sigma}_{12}\}. \tag{5.10}$$

The constant $\mathcal{U}$ is the complex (dimensionless) amplitude of the waves, $Kn\,St^2$ is the dimensionless frequency induced by the boundary conditions, and $\tilde{k}$ is the wave number.

After substitution of the harmonic solution into (5.7), it can be written as a homogeneous system,

$$\begin{bmatrix} i\,Kn\,St^2 & 0 & -i\,\tilde{k} \\ 0 & i\,Kn\,St^2 + \frac{2}{3}\frac{1}{Kn} + \frac{6}{5}\,Kn\,\tilde{k}^2 & -i\,\tilde{k} \\ -i\,\tilde{k} & -\frac{2}{5}\,i\,\tilde{k} & i\,Kn\,St^2 + \frac{1}{Kn} + \frac{16}{15}\,Kn\,\tilde{k}^2 \end{bmatrix} \begin{bmatrix} \tilde{v}_1 \\ \tilde{q}_1 \\ \tilde{\sigma}_{12} \end{bmatrix} = \begin{bmatrix} 0 \\ 0 \\ 0 \end{bmatrix}, \tag{5.11}$$

which serves as an equation for $\tilde{k}$. The dispersion relation, which relates $\tilde{k}$ and W, results from the requirement that the system (5.11) has nontrivial solutions, $\det[\cdot] = 0$. This gives two pairs of solutions with opposite signs, $\tilde{k} \in \{\tilde{k}_\ell(Kn, St), \ell = 1, 2, 3, 4\}$.

In order to relate the general solution to the boundary conditions, we write (5.10) as $\tilde{u}(\tilde{x}_2, \tilde{t}) = U(\tilde{x}_2) \exp(i\, Kn\, St^2\, \tilde{t})$ with $U = \{V_1, Q_1, \Sigma_{12}\}$. This form of the solution transforms the PDEs in (5.7) to the ODEs,

$$i\, Kn\, St^2\, V_1 + \frac{\mathrm{d}\Sigma_{12}}{\mathrm{d}\tilde{x}_2} = 0\,, \tag{5.12a}$$

$$i\, Kn\, St^2\, \Sigma_{12} + \frac{2}{5}\frac{\mathrm{d}Q_1}{\mathrm{d}\tilde{x}_2} + \frac{\mathrm{d}V_1}{\mathrm{d}\tilde{x}_2} - \frac{16}{15} Kn \frac{\mathrm{d}^2\Sigma_{12}}{\mathrm{d}\tilde{x}_2^2} = -\frac{1}{Kn}\Sigma_{12}\,, \tag{5.12b}$$

$$i\, Kn\, St^2\, Q_1 + \frac{\mathrm{d}\Sigma_{12}}{\mathrm{d}\tilde{x}_2} - \frac{6}{5} Kn \frac{\mathrm{d}^2 Q_1}{\mathrm{d}\tilde{x}_2^2} = -\frac{2}{3}\frac{1}{Kn} Q_1\,, \tag{5.12c}$$

which govern the amplitude distribution in the gas between the plates. Based on the solution of the dispersion relation (5.11), the solution for Σ_{12} is a superposition of the solutions

$$\Sigma_{12} = \sum_{\ell=1}^{4} \mathsf{C}_\ell \exp(-i\, \tilde{k}_\ell\, \tilde{x}_2), \tag{5.13a}$$

where the constants C_ℓ must be determined from boundary conditions. The solutions for velocity and heat-flux follow from (5.12) as

$$V_1 = -\frac{1}{i\, Kn\, St^2}\frac{\mathrm{d}\Sigma_{12}}{\mathrm{d}\tilde{x}_2}\,, \tag{5.13b}$$

$$Q_1 = -\frac{1}{i\, Kn\, St^2 + 2/(3\, Kn)}\left(\frac{6}{5} Kn \frac{\mathrm{d}^2 Q_1}{\mathrm{d}\tilde{x}_2^2} - \frac{\mathrm{d}\Sigma_{12}}{\mathrm{d}\tilde{x}_2}\right), \tag{5.13c}$$

with

$$\frac{\mathrm{d}Q_1}{\mathrm{d}\tilde{x}_2} = -\frac{5}{2}\left(\frac{1 + i\, Kn^2\, St^2}{Kn}\Sigma_{12} + \frac{\mathrm{d}V_1}{\mathrm{d}\tilde{x}_2}\right) + \frac{8}{3} Kn \frac{\mathrm{d}^2\Sigma_{12}}{\mathrm{d}\tilde{x}_2^2}.$$

Classical Case: The oscillatory Couette flow in the Navier–Stokes–Fourier system is simply described by the momentum equation (5.7a), in which after substitution of the law of Navier and Stokes (2.2) changes to the diffusion equation,

$$\frac{\partial \tilde{v}_1}{\partial \tilde{t}} = Kn \frac{\partial^2 \tilde{v}_1}{\partial \tilde{x}_2^2}. \tag{5.14}$$

The assumption of harmonic solution leads to an ODE for the velocity amplitude distribution

$$V_1 = \frac{1}{i\, St^2}\frac{\mathrm{d}^2 V_1}{\mathrm{d}\tilde{x}_2^2}, \tag{5.15}$$

with the general solution

$$V_1 = \mathsf{C}_1 \exp\left(\sqrt{i}\,\mathrm{St}\,\tilde{x}_2\right) + \mathsf{C}_2 \exp\left(-\sqrt{i}\,\mathrm{St}\,\tilde{x}_2\right). \tag{5.16}$$

Note that, unlike (5.3) and (5.6), in (5.13a) and (5.16) the exponential terms do not explicitly represent the Knudsen boundary layers. The constants C_1 and C_2 in the Navier–Stokes solutions will be determined from the velocity slip boundary condition.

5.4 Pulsating poiseuille flow

Similar to the unsteady Couette flow, for pulsating Poiseuille flow the time derivatives are retained, and additionally the oscillating body force is included. The linear equations read

$$\frac{\partial \tilde{v}_1}{\partial \tilde{t}} + \frac{\partial \tilde{\sigma}_{12}}{\partial \tilde{x}_2} = \tilde{G} \sin\left(W\,\tilde{t}\right), \tag{5.17a}$$

$$\frac{\partial \tilde{\sigma}_{12}}{\partial \tilde{t}} + \frac{2}{5}\frac{\partial \tilde{q}_1}{\partial \tilde{x}_2} + \frac{\partial \tilde{v}_1}{\partial \tilde{x}_2} - \frac{16}{15}\,Kn\frac{\partial^2 \tilde{\sigma}_{12}}{\partial \tilde{x}_2^2} = -\frac{1}{Kn}\tilde{\sigma}_{12}\,, \tag{5.17b}$$

$$\frac{\partial \tilde{q}_1}{\partial \tilde{t}} + \frac{\partial \tilde{\sigma}_{12}}{\partial \tilde{x}_2} - \frac{6}{5}Kn\frac{\partial^2 \tilde{q}_1}{\partial \tilde{x}_2^2} = -\frac{2}{3}\frac{1}{Kn}\tilde{q}_1, \tag{5.17c}$$

with two specific dimensionless parameters $\tilde{G}$ and W for the force amplitude and frequency. The dimensionless frequency W is defined by

$$W = \omega\, t_0 = \frac{\omega\, H}{\sqrt{\theta_0}} = Kn\, St^2, \tag{5.18}$$

and takes the role of the Stokes number in oscillatory Couette. Due to linearity, the velocity amplitude will be proportional to $\tilde{G}$. In the results below, we will choose $\tilde{G}$ such that for $Kn \to 0$ the velocity amplitude is unity, which requires $\tilde{G} = W$, since in this case $\sigma_{12} \to 0$ and $\partial_{\tilde{t}}\tilde{v}_1 = \tilde{G}\sin\left(W\,\tilde{t}\right)$. Accordingly, the continuum limit is a plug flow with $\tilde{v}_1 = \cos\left(W\,\tilde{t}\right)$ exhibiting a phase shift of $\pi/2$ with respect to the force.

For the solution, we will write the force in complex notation $\tilde{G}\exp\left(i\,W\,\tilde{t}\right)$. As above, general solutions are then expected as plane harmonic waves

$$\tilde{u}\left(\tilde{x}_2, \tilde{t}\right) = \mathcal{U}\exp\left[i\left(W\,\tilde{t} - \tilde{k}\,\tilde{x}_2\right)\right], \qquad \text{where} \qquad \tilde{u} = \{\tilde{v}_1, \tilde{q}_1, \tilde{\sigma}_{12}\}\,. \tag{5.19}$$

The linear system to determine the wave number $\tilde{k}$ is identical to (5.11), when substituting $Kn\,St^2$ by W. The solutions have the form $\tilde{k} \in \left\{\tilde{k}_\ell\left(Kn, W\right), \ell = 1, 2, 3, 4\right\}$. The final solution now includes the force

$$\Sigma_{12} = \sum_{\ell=1}^{4} \mathsf{C}_\ell \exp\left(-i\,\tilde{k}_\ell\,\tilde{x}_2\right), \tag{5.20a}$$

$$V_1 = \tilde{G} - \frac{1}{i\,\mathrm{W}}\frac{\partial \Sigma_{12}}{\partial \tilde{x}_2}\,, \tag{5.20b}$$

$$Q_1 = -\frac{1}{i\,\mathrm{W} + 2/(3Kn)}\left(\frac{6}{5}Kn\frac{\partial^2 Q_1}{\partial \tilde{x}_2^2} - \frac{\partial \Sigma_{12}}{\partial \tilde{x}_2}\right), \tag{5.20c}$$

with

$$\frac{\partial Q_1}{\partial \tilde{x}_2} = -\frac{5}{2}\left(\frac{1 + i\,\mathrm{W}Kn}{Kn}\Sigma_{12} + \frac{\partial V_1}{\partial \tilde{x}_2}\right) + \frac{8}{3}Kn\frac{\partial^2 \Sigma_{12}}{\partial \tilde{x}_2^2}.$$

6 Boundary conditions

The low-order moments which construct the Navier–Stokes–Fourier equations all have meaningful physical interpretations, and can be measured on the boundary. Experimental observations show that gases can slide over a surface, and that there can be a temperature inequality on the gas–surface interface. Such discontinuities in the equilibrium quantities on the boundary lie in the category of rarefaction effects, i.e., slip velocity and temperature jump. Typically, slip and jump are proportional to the Knudsen number.

In the Grad-type extended equations, e.g., the R13 equations, discontinuities on the boundary are extended to include the non-equilibrium quantities $\left\{\sigma_{ij}, q_i\right\}$. From the microscopic point of view, lack of sufficient collisions on the boundary leads to discontinuities in the particles' velocity distribution. Kinetic theory proves that the discontinuity in particles' velocity distribution is related to non-equilibrium effects, including Knudsen layers and jumps in the macroscopic quantities. It is also known that Knudsen layers contribute to the boundary jumps.

6.1 Boundary conditions for the R13 equations

Essentially, boundary conditions are jump conditions which link the wall velocity v_i^W and wall temperature θ_W to the gas properties adjacent to the wall. In theory, exact boundary conditions are available if the details of the gas–surface interaction are known. In the absence of such information, a simple argument going back to Maxwell [32] can be utilized to derive macroscopic boundary conditions for the moments. Accordingly, kinetic boundary conditions for the R13 equations [20,24] which are obtained from Maxwell's boundary condition for the Boltzmann equation (diffuse-reflection boundary condition) are used to solve the considered boundary value problems.

The full set of boundary conditions for two-dimensional flows, as depicted in Figs. 1 and 2, is [20]

$$\sigma_{12} = \frac{-\chi}{2-\chi}\sqrt{\frac{2}{\pi\theta}}\left(\mathcal{P}\mathcal{V}_1 + \frac{1}{5}q_1 + \frac{1}{2}m_{122}\right)n_2, \tag{6.1a}$$

$$q_2 = \frac{-\chi}{2-\chi}\sqrt{\frac{2}{\pi\theta}}\left(2\mathcal{P}\mathcal{T} - \frac{1}{2}\mathcal{P}\mathcal{V}^2 + \frac{1}{2}\theta\sigma_{22} + \frac{1}{15}\Delta + \frac{5}{28}R_{22}\right)n_2, \tag{6.1b}$$

$$R_{12} = \frac{\chi}{2-\chi}\sqrt{\frac{2}{\pi\theta}}\left(6\mathcal{P}\mathcal{T}\mathcal{V}_1 + \mathcal{P}\theta\mathcal{V}_1 - \mathcal{P}\mathcal{V}_1^3 - \frac{11}{5}\theta q_1 - \frac{1}{2}\theta m_{122}\right)n_2, \tag{6.1c}$$

$$m_{222} = \frac{\chi}{2-\chi}\sqrt{\frac{2}{\pi\theta}}\left(\frac{2}{5}\mathcal{P}\mathcal{T} - \frac{3}{5}\mathcal{P}\mathcal{V}^2 - \frac{7}{5}\theta\sigma_{22} + \frac{1}{75}\Delta - \frac{1}{14}R_{22}\right)n_2, \tag{6.1d}$$

$$m_{112} = \frac{-\chi}{2-\chi}\sqrt{\frac{2}{\pi\theta}}\left(\frac{1}{5}\mathcal{P}\mathcal{T} - \frac{4}{5}\mathcal{P}\mathcal{V}^2 + \frac{1}{14}R_{11} + \theta\sigma_{11} - \frac{1}{5}\theta\sigma_{22} + \frac{1}{150}\Delta\right)n_2, \tag{6.1e}$$

with the abbreviations

$$\begin{aligned}\mathcal{P} &= p + \frac{1}{2}\sigma_{22} - \frac{1}{120}\frac{\Delta}{\theta} - \frac{1}{28}\frac{R_{22}}{\theta},\\ \mathcal{V}_1 &= v_1 - v_1^W,\\ \mathcal{T} &= \theta - \theta_W.\end{aligned} \tag{6.2}$$

Velocity slip and temperature jump on the wall are $\mathcal{V}_1 = v_1 - v_1^W$ and $\mathcal{T} = \theta - \theta_W$, respectively. The surface accommodation factor is denoted by χ, and we set $\chi = 1$ in most cases, that is, we mainly consider fully diffusive boundaries. The wall normal vector is $\mathbf{n} = \{0, \pm 1, 0\}$, pointing to the gas, with $n_2 = +1$ for the lower wall (see Figs. 1–2).

For channel flows, the requirement that mass is conserved in the process gives an auxiliary condition,

$$\int_{-H/2}^{+H/2} \rho \, \mathrm{d}x_2 = \text{constant}. \tag{6.3}$$

In the present study, since we tackle the velocity problem, only the boundary conditions for the velocity problem are required, i.e., (6.1a, c), which in their linear form are

$$\tilde{\sigma}_{12} = \frac{-\chi}{2-\chi}\sqrt{\frac{2}{\pi}}\left(\tilde{\mathcal{V}}_1 + \frac{1}{5}\tilde{q}_1 + \frac{1}{2}\tilde{m}_{122}\right)n_2, \tag{6.4a}$$

$$\tilde{R}_{12} = \frac{\chi}{2-\chi}\sqrt{\frac{2}{\pi}}\left(\tilde{\mathcal{V}}_1 - \frac{11}{5}\tilde{q}_1 - \frac{1}{2}\tilde{m}_{122}\right)n_2. \tag{6.4b}$$

For the temperature and density problems Eqs. 6.1b, d and 6.1e, 6.3 are required, respectively.

Equation (6.4a) is the well-known slip condition for velocity, while in the same manner, Eq. 6.4b is the jump condition for parallel heat flux. In [18], these jump conditions are further discussed based on entropy generation on the boundary and the corresponding phenomenological relations.

6.2 Slip condition for Navier–Stokes–Fourier equations

It is straightforward to find the dimensionless slip velocity for the NSF equations from Eq. 6.4a, which after replacement of constitutive relations gives [21]

$$\tilde{v}_1^{(\mathrm{NSF})} = \frac{2-\chi}{\chi}\sqrt{\frac{\pi}{2}}\,Kn\,\alpha\,n_2 + \frac{1}{2}\,\beta - \frac{5}{6}\,Kn^2\,\frac{\partial\alpha}{\partial\tilde{x}_2}\,, \tag{6.5}$$

where α and β are our dimensionless velocity and temperature gradients, respectively. The first and second terms introduce first-order corrections to the no-slip condition, where $\beta/2$ is the thermal creep velocity for the BGK model (for Maxwell molecules the thermal creep velocity is $3\beta/4$). These first-order corrections come directly from the NSF constitutive relations, Eq. 2.2. The last term accounts for second-order contributions of $\tilde{q}_1$ and $\tilde{m}_{122}$ [21]. Different coefficients for this second-order correction are proposed in [21,33–35].

It is worth mentioning that in our half-space problems, second-order slip condition reduces to the first-order one, since the second-order derivative vanishes for the linear velocity functions, see the velocity solutions in (5.3) and (5.6).

7 Results

In this section, we provide comparison between our solutions to previously published data available in the literature as well as predictions for pulsating Poiseuille flow.

7.1 Kramer's problem (Viscous slip flow)

Velocity slip and defect in Kramer's problem have been extensively studied using kinetic approaches based on the Boltzmann equation [1,36–42].

The integrating constants $\mathsf{C}_1 - \mathsf{C}_4$ in Eq. 5.3 are determined from the boundary conditions (6.4) and (6.5) as

$$\mathsf{C}_1^{(\mathrm{R13})} = -Kn\,\alpha, \quad \mathsf{C}_2^{(\mathrm{R13})} = 0, \quad \mathsf{C}_3^{(\mathrm{R13})} = \frac{5\sqrt{\pi}\,Kn\,\alpha}{2\sqrt{35\pi} + 12\sqrt{2}\,\frac{\chi}{2-\chi}}, \quad \mathsf{C}_4^{(\mathrm{R13})} = \frac{2\pi\sqrt{35}\,\frac{2-\chi}{\chi} + 13\sqrt{2\pi}}{2\sqrt{70\pi} + 24\,\frac{\chi}{2-\chi}}\,Kn\,\alpha,$$

$$\mathsf{C}_1^{(\mathrm{NSF})} = -Kn\,\alpha, \quad \mathsf{C}_4^{(\mathrm{NSF})} = \frac{2-\chi}{\chi}\sqrt{\frac{\pi}{2}}\,Kn\,\alpha. \tag{7.1}$$

The constant C_1 follows from the bulk condition where the dimensionless velocity gradient is prescribed by $\partial_{\tilde{x}_2}\tilde{v}_1 = \alpha = 1$. Moreover, $\mathsf{C}_2 = 0$ results from the fact that the heat flux is finite in the far field.

Figure 3 shows the R13 and NSF solutions for velocity distribution in the viscous slip problem, i.e., Eq. 5.3. Solutions for different accommodation factors $\chi = \{0.2, 0.4, 0.6, 0.8, 1.0\}$ are presented, where the diamond symbols represent the BGK Boltzmann equation data of [37,42]. The Knudsen number and bulk velocity gradient in [37,42] are related to our definitions by $k = \sqrt{2}\,Kn$ and $\nu = \alpha$, respectively. In the plots, values for Knudsen number and velocity gradient are $Kn = 1/\sqrt{2}$ and $\alpha = 1$. In Fig. 3c profiles near the wall are magnified, where the effects of Knudsen boundary layers yield curvature in the velocity profiles. The NSF solution is a straight line, while the Knudsen layer in the R13 solution bends the bulk solution towards the Boltzmann solution. We observed a similar agreement when we compared our results with data in [40].

In [43], Kramer's problem is solved using several extended systems, including the R13 equations, where the exact boundary value from DSMC computations is forced on solutions of the macroscopic transport equations, and accuracy of the solutions are judged based on their bulk values. A similar comparison is conducted in [44]. Since the curvature of Knudsen boundary layers for the R13 equations is smaller than the actual curvature (from DSMC) this comparison procedure lets the R13 equations appear worse than they actually are. As Fig. 3 shows, the lack of curvature is compensated by extra slip, so that the R13 result matches the DSMC result in the bulk.

Knudsen layers in isothermal viscous slip flow, as given by the linear R13 equations, are depicted in Fig. 4. They construct the tangential heat flux, thus $\tilde{q}_1$ is a pure rarefaction effect. Larger accommodation factors, which yield more friction at the boundary, reduce the tangential heat flux.

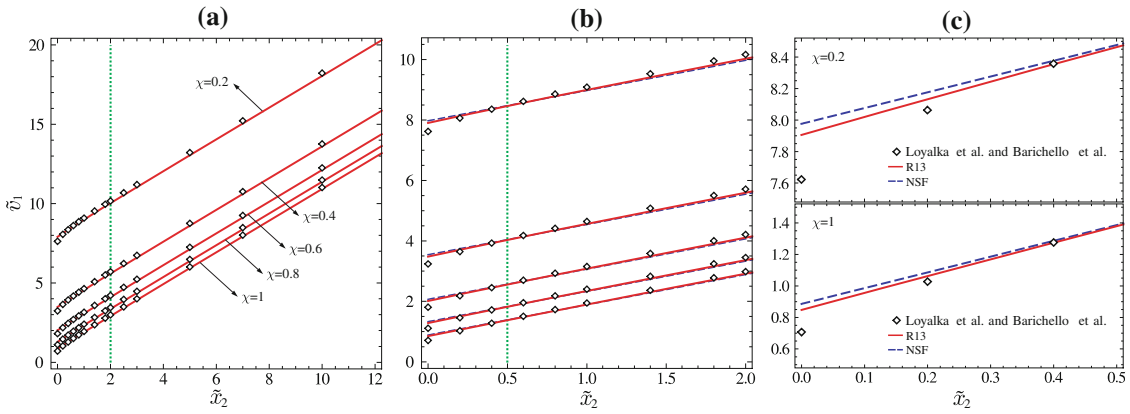

Fig. 3 Dimensionless velocity profiles in the viscous slip flow (Kramer's problem), obtained for different surface accommodation factors. Solution for the linearized NSF (*dashed blue line*) and linearized R13 (*continuous red line*) are compared to the linearized Boltzmann equation data (*diamonds*). Velocity distributions are shown within different distances from the wall. **a** For a large distance from the wall, NSF and R13 look identical, both correctly predict the bulk solution. **b, c** The same velocity profiles near the wall, where the Knudsen layers affect the profiles. Knudsen layers are absent in the Navier–Stokes–Fourier solution (*straight line*), while they introduce small curvature to the linear R13 solutions

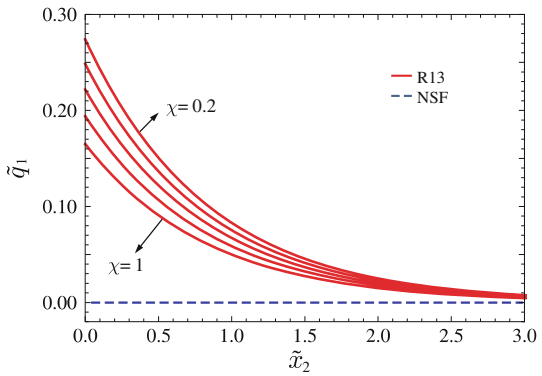

Fig. 4 Dimensionless parallel heat flux in the viscous slip flow (Kramer's problem), obtained for different surface accommodation factors. The streamwise heat flux is a pure rarefaction effect, thus, it only includes Knudsen layers. This streamwise heat flow which is not forced by temperature gradient is beyond the resolution of the classical NSF equations. Solutions for linearized NSF (*dashed blue line*) and linearized R13 (*continuous red line*) are presented

In Fig. 5, the coefficient C_4, which represents the viscous slip velocity, is plotted versus the accommodation factor. The viscous slip velocity does not include the Knudsen layer contribution to slip. The accurate evaluation of C_4 guaranties convergence of the solution to the bulk values. In the R13 system, the Knudsen layer bridges the boundary values to the bulk solution.

7.2 Thermal creep flow

Rarefaction effects in thermally driven flow over a surface, and transpiration flow in micro-channels are widely discussed in kinetic theory, see [25,37,40,42,45–50].

For the thermal creep flow the integrating constants $\mathsf{C}_1 - \mathsf{C}_4$ in Eq. 5.6 are determined from the boundary conditions (6.4) and (6.5) as

$$\mathsf{C}_1^{(\mathrm{R13})} = \mathsf{C}_2^{(\mathrm{R13})} = 0, \quad \mathsf{C}_3^{(\mathrm{R13})} = \frac{15\sqrt{2}\frac{\chi}{2-\chi}}{\sqrt{35\pi} + 6\sqrt{2}\frac{\chi}{2-\chi}} Kn\,\beta, \quad \mathsf{C}_4^{(\mathrm{R13})} = \frac{-\sqrt{35\pi}}{2\left(\sqrt{35\pi} + 6\sqrt{2}\frac{\chi}{2-\chi}\right)} Kn\,\beta,$$

$$\mathsf{C}_1^{(\mathrm{NSF})} = 0, \quad \mathsf{C}_4^{(\mathrm{NSF})} = \frac{1}{2}\,(1 - 2\,Kn)\,\beta, \tag{7.2}$$

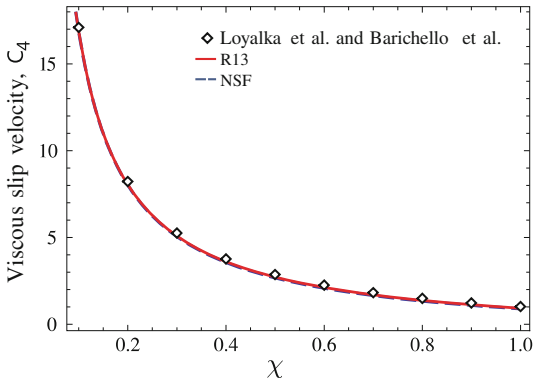

Fig. 5 Viscous slip velocity vs. momentum accommodation factor of the surface. Contribution of Knudsen boundary layers on slip velocity is not considered in the plot. Larger accommodation factors which represent rough surfaces, reduce the sliding velocity on the surface. The R13 and NSF systems predict the slip velocity with the same accuracy, which shows good agreement with Boltzmann equation data

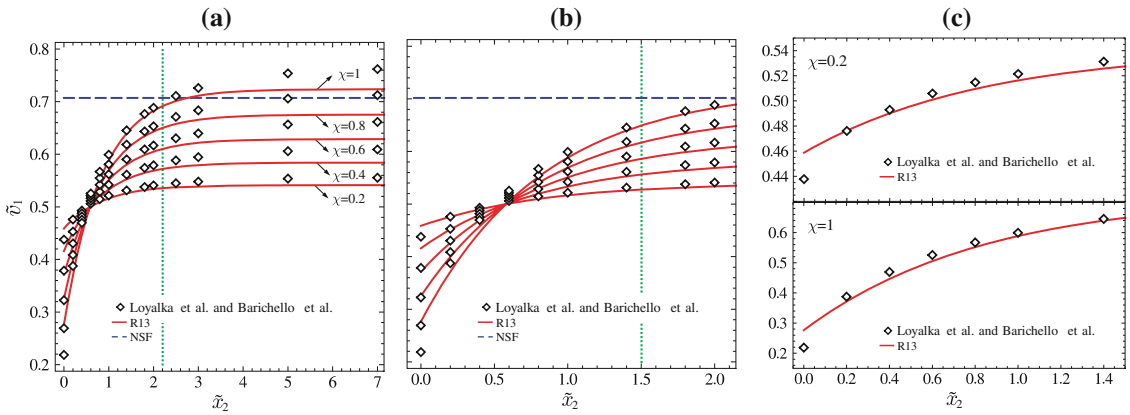

Fig. 6 Dimensionless velocity profiles in creep flow for different accommodation factors. Solutions for the linearized NSF (*dashed blue line*) and linearized R13 (*continuous red line*) are compared to linearized Boltzmann equation data (*diamonds*). Velocity distributions are shown within different distances from the wall. The NSF solution is a constant, which does not depend on the surface accommodation factor. **a** The bulk solution is predicted by the R13 equations with small error (about 3%). **b, c** The same velocity profiles near the wall, where the Knudsen layers affect the curvature of the profiles. Knudsen layers are absent in the constant Navier–Stokes–Fourier solution

In the bulk flow, the velocity distribution is uniform ($\partial_{\tilde{x}_2}\tilde{v}_1 = 0$) and the heat flux is finite. These conditions give $\mathsf{C}_1 = \mathsf{C}_2 = 0$ for the R13 solution.

For different accommodation factors, the creep velocities over the plate, as given by Eq. 5.6, are illustrated in Fig. 6. The Knudsen number and wall temperature gradient in [37,42] are related to our definitions by $\mathrm{k} = \sqrt{2}\,Kn$ and $\tau = \beta/\sqrt{2}$, respectively. In the plots values for Knudsen number and temperature gradient are $Kn = 1/\sqrt{2}$ and $\beta = \sqrt{2}$. For all accommodation factors NSF predicts a constant velocity (plug flow) since the slip condition (6.5) reduces to $\tilde{\mathcal{V}}_1^{(\mathrm{NSF})} = \beta/2$. R13, however, exhibits good agreement with the BGK Boltzmann data of [37,42]. As depicted in Fig. 6a, our simplified R13 model underestimates the bulk velocity specifically for diffusive walls. This difference might be addressed to the assumption of one-dimensional flow in our approach, or, to ambiguities in scaling the Boltzmann solutions. In Fig. 6b, c the velocity distribution near the wall is magnified; similar to Kramer's problem, Knudsen layers are visible.

In the creep flow, similar to the Kramer's problem, Knudsen layers appear in the tangential heat flux solution, Eq. 5.6. Figure 7 depicts the streamwise heat flux for both NSF and R13 systems. In the R13 solution, $\tilde{q}_1$ is a superposition of Knudsen layers and bulk solution (Fourier's law). Diffusive walls reduce the tangential heat flow at the boundary, however, they yield larger velocities in the bulk. Note that in creep flow heat and mass flow in opposite directions.

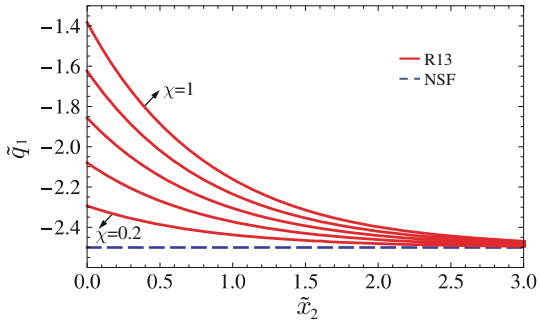

Fig. 7 Dimensionless parallel heat flux in the thermal creep flow, calculated for different surface accommodation factors. On NSF equations tangential heat flux is given by Fourier's law (*dashed blue line*), while in the R13 systems streamwise heat flux is a superposition of bulk solution (Fourier's law) and Knudsen boundary layers (*continuous red line*)

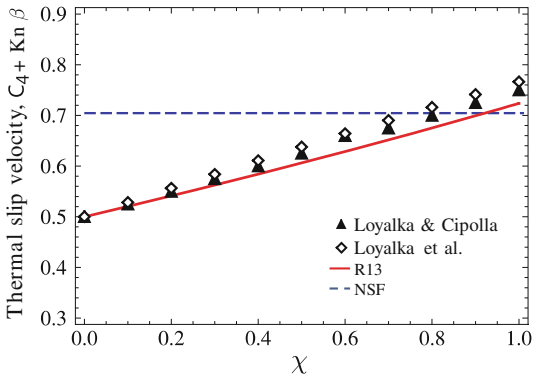

Fig. 8 Thermal slip velocity vs. momentum accommodation factor of the surface. Contribution of Knudsen boundary layers on slip velocity is not considered in the plot. In contrast to the viscous slip problem, larger accommodation factors which represent rough surfaces, increase the sliding velocity on the surface. The R13 gives outstanding agreement with the linearized Boltzmann equation data. The NSF solution is independent of surface accommodation coefficients and leads to a constant slip velocity

The constant C_4 versus accommodation factor is plotted in Fig. 8. As shown, in contrast to NSF the R13 system provides an acceptable estimate of the low speed thermal slip on the wall, compared to kinetic data in [37,45].

The assumption of one-dimensional velocity in thermally driven flow can be justified using the linear solutions (5.6) with the evaluated constants in (7.2). For two-dimensional steady flow the continuity equation can be written as

$$\tilde{\rho}\frac{\partial \tilde{v}_1}{\partial \tilde{x}_1} + \tilde{v}_1\frac{\partial \tilde{\rho}}{\partial \tilde{x}_1} + \frac{\partial \tilde{\rho}\tilde{v}_2}{\partial \tilde{x}_2} = 0,$$

where, according to the linear solution the first term is zero and the second one is of order β^2, since $-\partial_{\tilde{x}_1}\tilde{\rho} = \partial_{\tilde{x}_1}\tilde{\theta} = \beta$. Therefore, the last term should be of order β^2, and thus is zero in the linear limit. This argument gives $\tilde{\rho}\tilde{v}_2 =$ constant, and the boundary condition of impermeable walls yields $\tilde{v}_2 = 0$.

7.3 Oscillatory Couette flow

Figure 9 shows analytical solutions of linearized NSF and R13 for velocity and parallel heat flux. NSF solutions are given with both first- and second-order boundary conditions. Three pairs of Knudsen and Stokes numbers are selected within the transition regime to investigate the interaction of viscosity and rarefaction effects. The velocity solution is compared to DSMC data of [30].

Velocity plots show that as the gas becomes more rarefied, deviations of the macroscopic equations from the DSMC data increase at the boundaries, particularly at the oscillating boundary. The differences between NSF and R13 are small, but the R13 solutions are more accurate at higher Knudsen numbers. In general, the

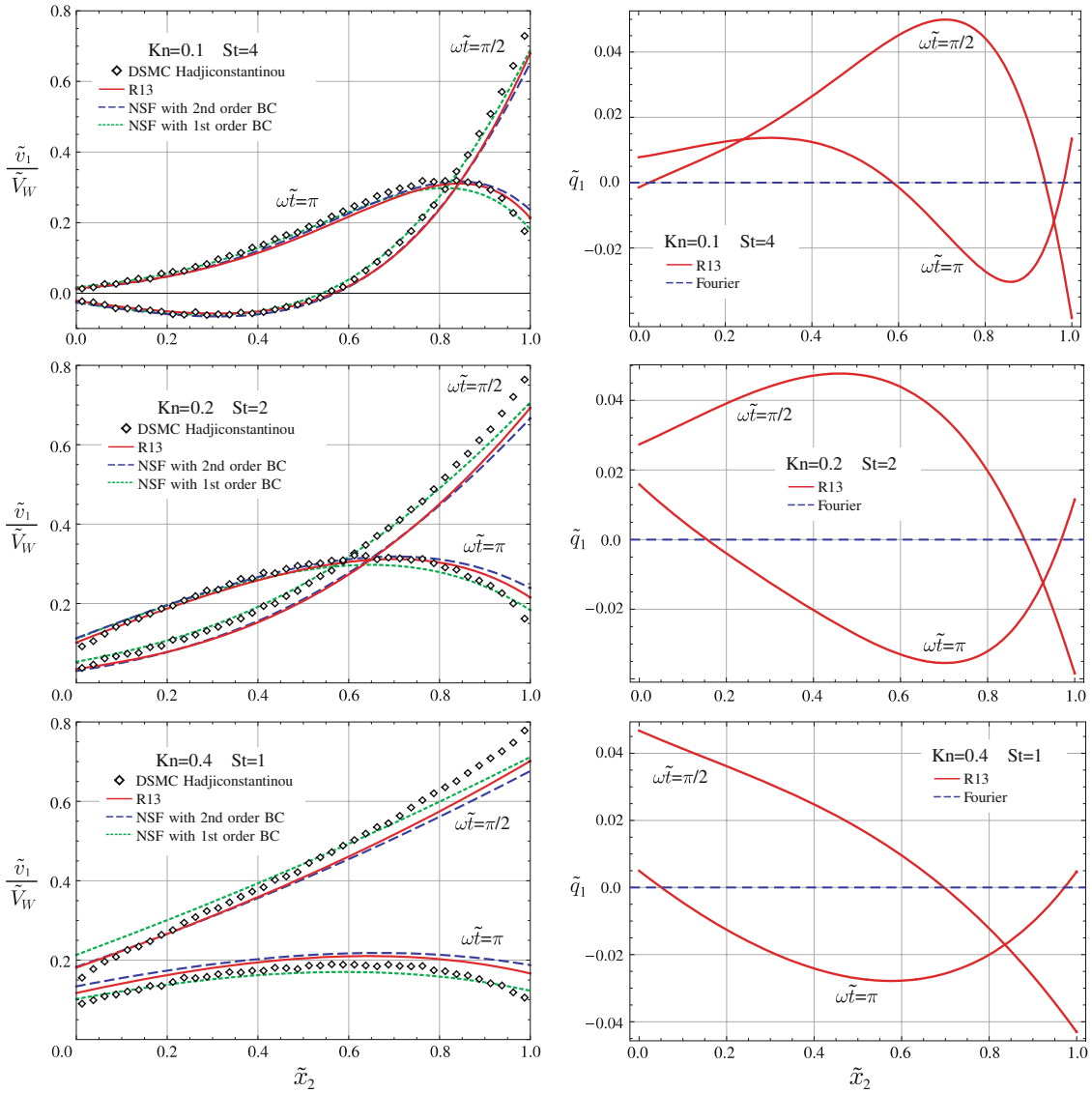

Fig. 9 Interaction between rarefaction and viscosity effects in oscillatory Couette flow are illustrated using three pairs of Knudsen–Stokes numbers at $\omega\tilde{t} = \{\pi, \pi/2\}$. *Left* Analytical velocity solutions for Navier–Stokes–Fourier and regularized 13-moment equations are compared to direct simulation Monte Carlo data. *Right* Oscillatory Knudsen layers (parallel heat flow) which are zero in Navier–Stokes–Fourier are presented for linear R13 equations

solution that gives the required curvature at the boundary, and sooner converges to the bulk solution must be considered as the best solution. At the first glance, the NSF solution with the first-order slip condition seems to be very close to the DSMC data. NSF behaves better right on the surface, but due to the lack of Knudsen layers, it under-estimates the curvature and then converges to the bulk solution in a longer distance, compared to the R13 solution, especially for the case of small Knudsen numbers. Second-order slip condition improves the curvature on the boundary such that its bulk solution becomes close to the R13 bulk solution.

Near the oscillating boundary, the curvature of R13 differs from NSF due to Knudsen layers, i.e., parallel heat flux. The Knudsen layers are shown in the left plots of Fig. 9, which are zero in NSF theory.

Our linear approach treats viscosity as a constant, i.e., independent of temperature. Indeed, dependence of viscosity on temperature covers a portion of non-linear effects, which are excluded in the presented calculations. This can be addressed as the most likely reason for differences between the DSMC and analytical results.

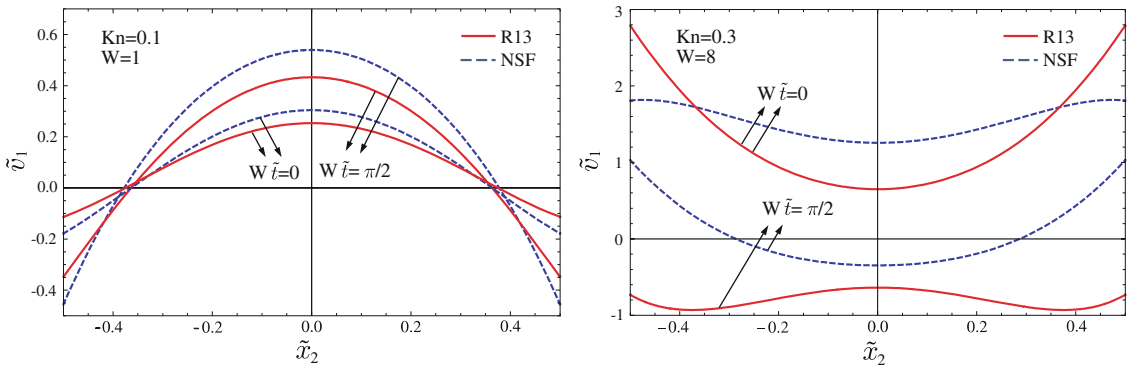

Fig. 10 Comparison of velocity profiles for pulsating Poiseuille flow computed with NSF and R13 for two different situations: ($W = 1$, $Kn = 0.1$) and ($W = 8$, $Kn = 0.3$). The plots show the two different times $W\tilde{t} = 0$ and $W\tilde{t} = \pi/2$ within one force cycle

7.4 Pulsating poiseuille flow

For pulsating Poiseuille flow, DSMC or experimental data could not be found for large Knudsen numbers. Here, we present the results for the linearized NSF and R13 systems, and demonstrate that large deviations between the models are possible, even for moderate Knudsen numbers. The results for NSF have been computed with full second-order slip boundary conditions.

Figure 10 displays the velocity profiles for two different cases, and two time instances $W\tilde{t} = 0$, and $W\tilde{t} = \pi/2$ within one cycle of the oscillating force. The left plot of the figure uses $Kn = 0.1$ and a dimensionless frequency of $W = 1$. Both results show qualitative agreement, but NSF somewhat overestimates the velocity value in the middle of the channel. The right plot of the figure displays the result for $Kn = 0.3$ and $W = 8$, that is for a 8-times higher frequency. The differences between NSF and R13 are marked.

In order to obtain more insight into the behavior of the solutions for pulsating Poiseuille flow, we compute the average velocity

$$\int_{-1/2}^{1/2} v_1\left(\tilde{x}_2, \tilde{t}\right) d\tilde{x}_2 = \mathcal{A}\,\sin\left(W\tilde{t} + \gamma\right), \tag{7.3}$$

with amplitude $\mathcal{A}$ and phase shift γ. This quantity depends only on Knudsen number and frequency W, but not on space and time. In Fig. 11, we plot the amplitude and phase shift as functions of Kn for two frequencies, $W = 1$ (upper plots), and $W = 8$ (lower plots).

For very small Knudsen number the amplitude converges to $\mathcal{A} = 1$ and the phase shift becomes $\gamma = \pi/2$, due to the scaling of the force as mentioned above. For larger Knudsen numbers the amplitude and phase shift follow rather complicated curves reflecting the complex interplay of convection, dissipation and boundary conditions in the process.

The case $W = 1$ shows differences between NSF and R13 only for relatively large Knudsen numbers, especially in the phase shift. Note that independent of W the phase shift converges to $\gamma = \pi/2$ for large Knudsen numbers for both models. For the larger frequency $W = 8$ the differences are already very strong for Knudsen numbers as small as $Kn = 0.1$. The NSF equations predict a phase shift smaller than or roughly $\pi/2$ while R13 gives clearly $\gamma > \pi/2$ in the range $0.05 < Kn < 1.0$. Similarly, the amplitude shows much larger values in the NSF result. Due to the higher accuracy of R13 for larger Knudsen numbers and faster processes, we expect the R13 result to be superior over the NSF solution. It remains to compare amplitude and phase shift to DSMC solutions or experimental data for pulsating Poiseuille flow.

8 Conclusions

In the present study, we examined the capabilities of Navier–Stokes–Fourier with second-order slip condition, and regularized 13-moment equations to describe common boundary value problems of gas dynamics. A characteristic feature of the selected boundary value problems is the formation of Knudsen layers on the boundary.

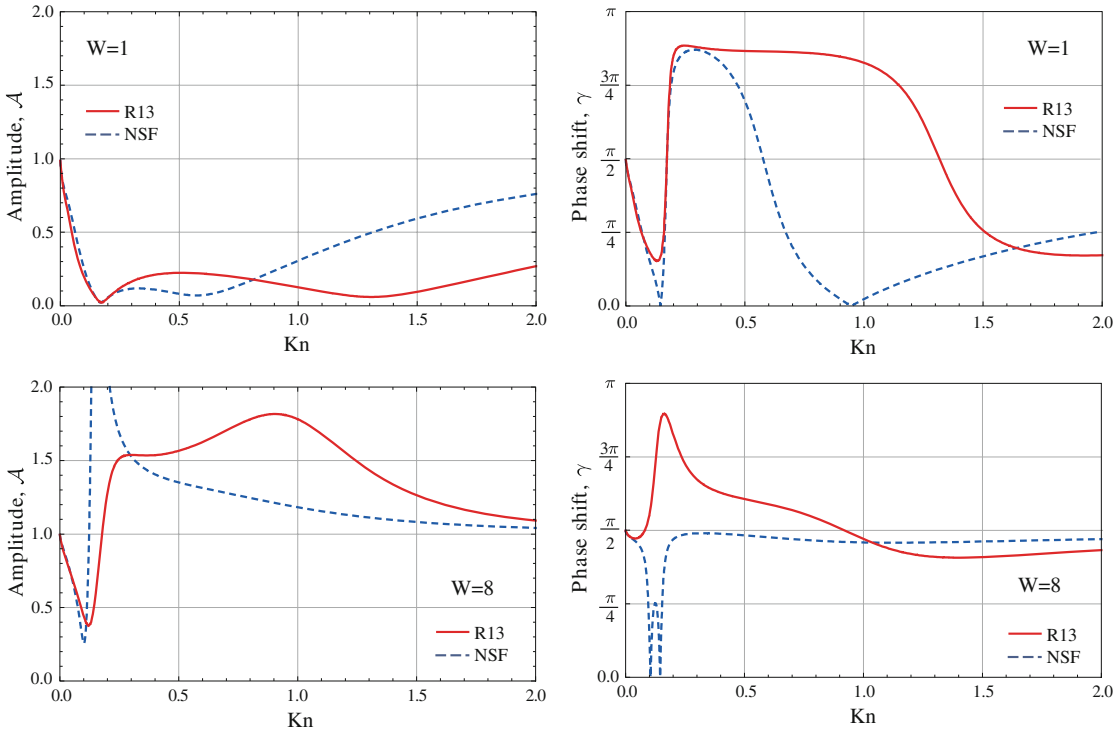

Fig. 11 Amplitude and phase shift of velocity over Knudsen number in pulsating Poiseuille flow for NSF and R13. This figure shows the frequencies $W = \{1, 8\}$ and uses accommodation factor $\chi = 1$. Phase shift converges to $\pi/2$ for large Kn both for NSF and R13. For high-frequency flow $W = 1$, the models predict opposite phase shifts for $Kn \approx 0.2$

Flows in the linear regime were considered, which allows to neglect the coupling of velocity and temperature fields.

We showed by means of analytical solutions that the classical Navier–Stokes–Fourier equations are unable to capture the Knudsen boundary layers, however, higher-order boundary conditions enable them to predict the slip velocity, which also provides correction to the bulk values. In Kramer's problem, differences between NSF and R13 are important in rarefied conditions, where the length scale is comparable to the Knudsen layer thickness, e.g., micro Couette flows or high-altitude flights. For thermally induced flows, linearized NSF cannot predict the flow pattern and its dependence to the boundary accommodation; it gives a constant bulk velocity and velocity slip. In the unsteady flows, where rarefaction and unsteady effects interact, NSF with second-order slip condition yields acceptable results in the transition regime, which are comparable with the R13 results. The next step is to develop a damping model for MEMS application, based on R13 equations.

For pulsating Poiseuille flow NSF and R13 behave quite differently, particularly, in the phase shift. The results must be interpreted as prediction for this type of flows.

In conclusion, advantages of R13 over NSF are highlighted in both steady and unsteady problems. Historical background and simplicity of Navier–Stokes and Fourier equations are their welcoming feature, which makes them popular in the engineering community. It is shown that R13 equations and the corresponding boundary conditions can be used as a higher-order alternative for NSF, to provide more accurate solutions for rarefied gas dynamics problems.

Acknowledgments This research was supported by the Natural Sciences and Engineering Council (NSERC), and the European Science Foundation (ESF).

Appendix: Regularized 13-moment equations for BGK kinetic model

For the Bhatnagar–Groos–Krook (BGK) model [51], the R13 equations bear different factors. Particularly, the heat flux balance (2.3) and constitutive equations (2.5) change to [13]

$$\frac{\partial q_i}{\partial t} + \cdots - \frac{\sigma_{ij}}{\rho}\frac{\partial \sigma_{jk}}{\partial x_k} = -\frac{p}{\mu} q_i, \tag{A.1}$$

and

$$\begin{aligned} \Delta &= -\frac{\sigma_{ij}\sigma_{ij}}{\rho} - 8\frac{\mu}{p}(\ldots), \\ R_{ij} &= -\frac{4}{7}\frac{\sigma_{k\langle i}\sigma_{j\rangle k}}{\rho} - \frac{28}{5}\frac{\mu}{p}(\ldots), \\ m_{ijk} &= -3\frac{\mu}{p}(\ldots), \end{aligned} \tag{A.2}$$

where the dots stand for their counterparts in (2.3) and (2.5).
Similarly, the Fourier's law changes to

$$q_i^{(\text{NSF-BGK})} = -\frac{5}{2}\mu\frac{\partial \theta}{\partial x_i}, \tag{A.3}$$

since the BGK model gives the Prandtl number as unity, $Pr = 1$.

References

1. Cercignani, C.: Theory and application of the Boltzmann equation. Scottish Academic Press, Edinburgh (1975)
2. de Groot, S.R., Mazur, P.: Non-equilibrium thermodynamics. Dover, New York (1984)
3. Chapman, S., Cowling, T.G.: The mathematical theory of non-uniform gases. Cambridge University Press, Cambridge (1970)
4. Grad, H.: On the kinetic theory of rarefied gases. Commun. Pure Appl. Math. **2**, 331–407 (1949)
5. Grad, H.: Principles of the kinetic theory of gases. In: Flügge, S. (ed.) Handbuch der Physik, Springer, Berlin (1958)
6. Bobylev, A.V.: The Chapman-Enskog and Grad methods for solving the Boltzmann equation. Sov. Phys. Dokl. **27**, 29–31 (1982)
7. Rosenau, P.: Extending hydrodynamics via the regularization of the Chapman-Enskog expansion. Phys. Rev. A **40**, 7193–7196 (1989)
8. Zhong, X., MacCormack, R.W., Chapman, D.R.: Stabilization of the Burnett equations and applications to hypersonic flows. AIAA J. **31**, 1036–1043 (1993)
9. Jin, S., Slemrod, M.: Regularization of the Burnett equations via relaxation. J. Stat. Phys. **103**, 1009–1033 (2001)
10. Müller, I., Reitebuch, D., Weiss, W.: Extended thermodynamics—consistent in order of magnitude. Contin. Mech. Thermodyn. **15**, 113–146 (2003)
11. Bobylev, A.V.: Instabilities in the Chapman-Enskog expansion and Hyperbolic Burnett equations. J. Stat. Phys. **124**, 371–399 (2006)
12. Söderholm, L.H.: Hybrid Burnett Equations: a new method of stabilizing. Transp. Theory Stat. Phys. **36**, 495–512 (2007)
13. Struchtrup, H.: Macroscopic transport equations for rarefied gas flows. Vol. XII, Springer, New York (2005)
14. Struchtrup, H., Torrilhon, M.: Regularization of Grad's 13-moment equations: derivation and linear analysis. Phys. Fluids **15**, 2668–2680 (2003)
15. Struchtrup, H.: Stable transport equations for rarefied gases at high orders in the Knudsen number. Phys. Fluids **16**, 3921–3934 (2004)
16. Torrilhon, M., Struchtrup, H.: Regularized 13-moment-equations: shock structure calculations and comparison to Burnett models. J. Fluid Mech. **513**, 171–198 (2004)
17. Struchtrup, H., Thatcher, T.: Bulk equations and Knudsen layers for the regularized 13 moment equations. Contin. Mech. Thermodyn. **19**, 177–189 (2007)
18. Struchtrup, H., Torrilhon, M.: H theorem, regularization, and boundary conditions for linearized 13-moment equations. Phys. Rev. Lett. **99**, 014502 (2007)
19. Struchtrup, H.: Linear kinetic heat transfer: moment equations, boundary conditions, and Knudsen layers. Phys. A **387**, 1750–1766 (2008)
20. Torrilhon, M., Struchtrup, H.: Boundary conditions for regularized 13-moment-equations for micro-channel-flows. J. Comput. Phys. **227**, 1982–2011 (2008)
21. Struchtrup, H., Torrilhon, M.: High order effects in rarefied channel flows. Phys. Rev. E **78**, 046301 (2008)
22. Taheri, P., Torrilhon, M., Struchtrup, H.: Couette and Poiseuille microflows: analytical solutions for regularized 13-moment equations. Phys. Fluids **21**, 017102 (2009)
23. Taheri, P., Struchtrup, H.: Rarefaction effects in thermally-driven microflows (2009, submitted)

24. Gu, X.J., Emerson, D.R.: A computational strategy for the regularized 13-moment equations with enhanced wall-boundary conditions. J. Comput. Phys. **225**, 263–283 (2007)
25. Ohwada, T., Sone, Y., Aoki, K.: Numerical analysis of the Poiseuille and thermal transpiration flows between two parallel plates on the basis of the Boltzmann equation for hard-sphere molecules. Phys. Fluids A **1**, 2042–2049 (1989)
26. Landau, L.D., Lifshitz, E.M.: Fluid mechanics. Pergamon, Oxford (1987)
27. Gad-el-Hak, M. (ed.): The MEMS handbook: introduction and fundamentals. CRC, London (2005)
28. Bahukudumbi, P., Park, J.H., Beskok, A.: A unified engineering model for steady and quasi-steady shear-driven gas microflows. Microscale Thermophys. Eng. **7**, 291–315 (2003)
29. Park, J.H., Bahukudumbi, P., Beskok, A.: Rarefaction effects on shear driven oscillatory gas flows: A direct simulation Monte Carlo study in the entire Knudsen regime. Phys. Fluids **16**, 317–330 (2004)
30. Hadjiconstantinou, N.G.: Oscillatory shear-driven gas flow in the transition and free-molecular-flow regimes. Phys. Fluids **17**, 100611 (2005)
31. Sharipov, F., Kalempa, D.: Oscillatory Couette flow at arbitrary oscillation frequency over the whole range of the Knudsen number. Microfluid. Nanofluid. **4**, 363–374 (2008)
32. Maxwell, J.C.: On stresses in rarefied gases arising from inequalities of temperature. Philos. Trans. R. Soc. Lond. **170**, 231–256 (1879)
33. Lockerby, D.A., Reese, J.M., Emerson, D.R., Barber, R.W.: Velocity boundary condition at solid walls in rarefied gas calculations. Phys. Rev. E **70**, 017303 (2004)
34. Deissler, R.G.: An analysis of second order slip flow and temperature jump boundary conditions for rarefied gases. Int. J. Heat Mass Transf. **7**, 681–694 (1964)
35. Hadjiconstantinou, N.G.: Comment on Cercignani's second-order slip coefficient. Phys. Fluids **15**, 2352–2354 (2003)
36. Loyalka, S.K.: Velocity profile in the Knudsen layer for the Kramer's problem. Phys. Fluids **18**, 1666–1669 (1975)
37. Loyalka, S.K., Petrellis, N., Storvick, T.S.: Some numerical results for the BGK model: thermal creep and viscous slip problems with arbitrary accommodation at the surface. Phys. Fluids **18**, 1094–1099 (1975)
38. Loyalka, S.K., Ferziger, H.: Model dependence of the slip coefficient. Phys. Fluids **10**, 1833–1839 (1967)
39. Loyalka, S.K., Hickey, K.A.: Velocity slip and defect: hard sphere gas. Phys. Fluids A **1**, 612–614 (1989)
40. Ohwada, T., Sone, Y., Aoki, K.: Numerical analysis of the shear and thermal creep flows of a rarefied gas over a plane wall on the basis of the linearized Boltzmann equation for hard-sphere molecules. Phys. Fluids A **1**, 1588–1599 (1989)
41. Loyalka, S.K., Hickey, K.A.: The Kramers problem: velocity slip and defect for a hard sphere gas with arbitrary accommodation. J. Appl. Math. Phys. (ZAMP) **41**, 245–253 (1990)
42. Barichello, L.B., Camargo, M., Rodrigues, P., Siewert, C.E.: Unified solutions to classical flow problems based on the BGK model. Z. Angew. Math. Phys. (ZAMP) **52**, 517–534 (2001)
43. Lockerby, D.A., Reese, J.M., Gallis, M.A.: The usefulness of higher-order constitutive relations for describing the Knudsen layer. Phys. Fluids **17**, 100609 (2005)
44. Lilley, C.R., Sader, J.E.: Velocity gradient singularity and structure of the velocity profile in the Knudsen layer according to the Boltzmann equation. Phys. Rev. E **76**, 026315 (2007)
45. Loyalka, S.K., Cipolla, J.W.: Thermal creep slip with arbitrary accommodation at the surface. Phys. Fluids **14**, 1656–1661 (1971)
46. Kanki, T., Iuchi, S.: Poiseuille flow and thermal creep of a rarefied gas between parallel plates. Phys. Fluids **16**, 594–599 (1973)
47. Loyalka, S.K.: Comments on Poiseuille flow and thermal creep of a rarefied gas between parallel plates. Phys. Fluids **17**, 1053–1055 (1974)
48. Loyalka, S.K., Petrellis, N., Storvick, T.S.: Some exact numerical results for the BGK model: Couette, Poiseuille and thermal creep flow between parallel plates. Z. Angew. Math. Phys. (ZAMP) **30**, 514–521 (1979)
49. Loyalka, S.K.: Temperature jump and thermal creep slip: rigid sphere gas. Phys. Fluids **A1**, 403–408 (1989)
50. Sone, Y.: Kinetic theory and fluid dynamics. Birkhäuser, Boston (2002)
51. Bhatnagar, P.L., Gross, E.P., Krook, M.: A model for collision processes in gases. I. Small amplitude processes in charged and neutral one-component systems. Phys. Rev. **94**, 511–525 (1954)